Acta Biomaterialia 23 (2015) S3–S15

Contents lists available at ScienceDirect

Acta Biomaterialia

journal homepage: www.elsevier.com/locate/actabiomat

Reprint of: Connections between single-cell biomechanics and human disease states: gastrointestinal cancer and malaria

S. Suresh [a,b,*], J. Spatz [c], J.P. Mills [a], A. Micoulet [c], M. Dao [a], C.T. Lim [d], M. Beil [e], T. Seufferlein [e]

[a] Department of Materials Science and Engineering, and Division of Bioengineering, Massachusetts Institute of Technology, Room 8-309, 77 Massachusetts Ave., Cambridge, MA 02139-4307, USA
[b] Division of Biological Engineering and Affiliated Faculty of the Harvard-MIT Division of Health Sciences and Technology, Cambridge, MA 02139-4307, USA
[c] Institute for Physical Chemistry, Biophysical Chemistry, University of Heidelberg, INF 253, 69120 Heidelberg, Germany
[d] Division of Bioengineering and Department of Mechanical Engineering, National University of Singapore, Singapore 117576, Singapore
[e] Department of Internal Medicine I and Department of Physical Chemistry, University of Ulm, 89071 Ulm, Germany

ARTICLE INFO

Article history:
Received 13 July 2004
Received in revised form 2 September 2004
Accepted 2 September 2004

Keywords:
Epithelial cells
Human red blood cells
Mechanical properties
Gastrointestinal cancer
Malaria

ABSTRACT

We investigate connections between single-cell mechanical properties and subcellular structural reorganization from biochemical factors in the context of two distinctly different human diseases: gastrointestinal tumor and malaria. Although the cell lineages and the biochemical links to pathogenesis are vastly different in these two cases, we compare and contrast chemomechanical pathways whereby intracellular structural rearrangements lead to global changes in mechanical deformability of the cell. This single-cell biomechanical response, in turn, seems to mediate cell mobility and thereby facilitates disease progression in situations where the elastic modulus increases or decreases due to membrane or cytoskeleton reorganization. We first present new experiments on elastic response and energy dissipation under repeated tensile loading of epithelial pancreatic cancer cells in force- or displacement-control. Energy dissipation from repeated stretching significantly increases and the cell's elastic modulus decreases after treatment of Panc-1 pancreatic cancer cells with sphingosylphosphorylcholine (SPC), a bioactive lipid that influences cancer metastasis. When the cell is treated instead with lysophosphatidic acid, which facilitates actin stress fiber formation, neither energy dissipation nor modulus is noticeably affected. Integrating recent studies with our new observations, we ascribe these trends to possible SPC-induced reorganization primarily of keratin network to perinuclear region of cell; the intermediate filament fraction of the cytoskeleton thus appears to dominate deformability of the epithelial cell. Possible consequences of these results to cell mobility and cancer metastasis are postulated. We then turn attention to progressive changes in mechanical properties of the human red blood cell (RBC) infected with the malaria parasite *Plasmodium falciparum*. We present, for the first time, continuous force–displacement curves obtained from in-vitro deformation of RBC with optical tweezers for different intracellular developmental stages of parasite. The shear modulus of RBC is found to increase up to 10-fold during parasite development, which is a noticeably greater effect than that from prior estimates. By integrating our new experimental results with published literature on deformability of *Plasmodium*-harbouring RBC, we examine the biochemical conditions mediating increases or decreases in modulus, and their implications for disease progression. Some general perspectives on connections among structure, single-cell mechanical properties and biological responses associated with pathogenic processes are also provided in the context of the two diseases considered in this work.

1. Introduction

Many cellular functions, such as cell division, motility, gene expression, signal transduction, wound healing and apoptosis (programmed cell death), critically depend on mediation and regulation of stress as well as elastic and viscoelastic properties of cell membrane and intracellular proteins and fluid (e.g., [1–3]). The

This article is a reprint of a previously published article. For citation purposes, please use the original publication details; Acta Biomater. 1 (2005) 15–30.
DOI of original article: http://dx.doi.org/10.1016/j.actbio.2004.09.001
* Corresponding author. Address: Department of Materials Science and Engineering, and Division of Bioengineering, Massachusetts Institute of Technology, Room 8-309, 77 Massachusetts Ave., Cambridge, MA 02139-4307, USA. Tel.: +1 617 253 3320
E-mail address: ssuresh@mit.edu (S. Suresh).

http://dx.doi.org/10.1016/j.actbio.2015.07.015
1742-7061/

changes in the elastic and viscoelastic properties of living cells are also linked strongly to the manner in which the cells respond to structural and molecular alterations induced by the onset and progression of diseases and to invasion by foreign organisms, such as parasites (e.g., [4–7]). Such changes in mechanical response are also known to play key roles in pathogenesis and pathophysiology [2,6,7].

The elastic modulus of a living cell can either increase or decrease depending on the biochemical origins of molecular reorganization occurring in conjunction with the developmental stages of pathogenic processes (e.g., [8]). Molecular architecture, transport properties and mechanical responses of the cytoskeleton, which is a dense intracellular biopolymeric network, are mediated and regulated by associated proteins. Strong chemomechanical coupling elicits reactions from the cytoskeleton [9]. For example, cellular signalling generated by surface recognition via integrins can cause a series of biochemical reactions which, in turn, lead to precise control and regulation of cytoskeleton structure, effective elastic response of the cell and its adhesion properties. In many cases, changes to cytoskeleton structure and mechanical properties are also accompanied by changes in cell shape and mobility [10]. Understanding the mechanisms associated with the connections among molecular reorganization in diseased cells and the resultant changes to the mechanical properties can, therefore, be critical to developing a complete knowledge of the developmental processes underlying disease progression.

Advances in experimental biophysics and bioengineering in the past two decades have enabled direct, real-time mechanical probing and manipulation of single cells and molecules. Such methods are now capable of imposing and sensing forces and displacements with resolutions as fine as a picoNewton and a nanometer, respectively, in a well-controlled manner. Available experimental techniques to probe single cells include micropipette aspiration, optical tweezers (also known as optical or laser traps), magnetic tweezers, atomic/molecular force probes, nanoindenters, microplate manipulators and optical stretchers. Descriptions of these techniques can be found in recent reviews [2,5,11–17].

In this paper, we explore connections among molecular structure of the cytoskeleton, cellular and subcellular elastic response, and human disease states. For this purpose, we consider experimental observations of single-cell mechanics associated with two very different human diseases: gastrointestinal tumor and malaria induced by the parasite *Plasmodium falciparum*. By integrating new experimental observations presented in this paper with our recent results [16,17], we identify critical elements of the structure–property–function connections underlying single-cell mechanical response in the context of these diseases. For the two disease states examined, we focus on the biochemical conditions for which the elastic modulus of the affected cell can either increase or decrease in the diseased state as compared to the healthy cell. We link, wherever possible, such changes in mechanical response with the underlying changes in molecular architecture as a consequence of disease development and to changes in cell shape and mobility. We further describe how such differences in alterations to mechanical properties regulate different biological and physiological responses during the developmental stages of the disease.

The paper is arranged in the following sequence. Section 2 deals with the single-cell mechanics of epithelial pancreatic cancer cells (Panc-1). We first present new experimental observations, obtained under physiological conditions (37 °C, 5% CO_2-containing air), of force-controlled and displacement-controlled tensile loading of single Panc-1 cell, using the microplate mechanical stretcher method [14–16]. These results illustrate how specific biochemical factors either increase or decrease the elastic stiffness. Results of evolution of hysteretic energy dissipation from force–displacement loops during repeated tensile cycling of the cell under force-control and displacement-control are also obtained so as to examine possible effects of biochemical factors. We then examine the underlying reorganization of molecular assembly in response to controlled biochemical modifications. Possible links among such structure and property changes and metastasis are postulated. Section 3 deals with another very different process that can lead to disease state involving human red blood cells (RBCs) parasitized by *Plasmodium* (*P.*) *falciparum* malaria parasites. Here the effects of infestation on the mechanical response of the single cell are investigated in vitro by recourse to direct large deformation tensile stretching with optical tweezers. Direct force–displacement curves are described for the first time for different developmental stages of the parasite inside the RBC and the results are compared with similar experiments performed on reference conditions involving healthy RBCs and uninfected RBCs exposed to the parasite. This information is then combined along with three-dimensional computational simulations of optical tweezers stretching to demonstrate how parasitization causes a marked increase in elastic stiffness.[1] Possible causes of this stiffening arising from transport of specific proteins from the parasite to the cell membrane or cytoskeleton are described. Micromechanical assays of RBCs parasitized by *P. falciparum* using the present optical tweezers studies are compared with those from other independent experimental methods [8,18], and the differing effects on mechanical response of RBCs from infestation by different parasites, viz., *P. falciparum* and *P. vivax*, are addressed. The paper concludes with some general perspectives on possible connections among mechanical properties, intracellular molecular reorganization and disease characteristics in the context of the differing situations involving gastrointestinal epithelial cancer and malaria.

2. Mechanics of human Panc-1 pancreatic cancer cells

Cytoskeletal components of human epithelial cells include filamentous biopolymers such as actin, microtubules and intermediate filaments. About 5% of the total protein structure of epithelial cells comprises keratins which are organized into biomolecular bundles, constituting chiefly the intermediate filaments of the cells and determining the mechanical characteristics of the cytoplasm. While human pancreatic cancer[2] cells express keratins 7, 8, 18 and 19, the subline of Panc-1 cells are known to express primarily K8 and K18.

2.1. Effects of SPC on the subcellular structure of Panc-1 cells

Sphingosylphosphorylcholine (SPC) is a bioactive lipid which promotes anti-apoptotic effects in human blood components such as blood plasma and high density lipoprotein (HDL) particles where it occurs naturally [19]. Elevated levels of SPC are also found in the brains of people afflicted with type A form of Niemann–Pick disease [20] (which is an inherited metabolic disorder caused by the accumulation of a fatty substance in the spleen, liver, lungs, bone marrow, or brain) and in blood and malignant ascites of ovarian cancer patients [21]. Because of its propensity to mediate cell proliferation [22] and cell migration [23], SPC is also considered to play a key role in cancer metastasis.

[1] Details of materials and experimental and computational methods used to obtain the results reported in both Sections 2 and 3 are summarized in the supplementary material accompanying this paper in the journal website.

[2] The human pancreas serves to accomplish two major functions: secretion of pancreatic juice into the duodenum along the pancreatic duct and regulation of blood glucose levels by secreting insulin and glucagons. Cancer of the pancreas is one of the leading causes of death due to cancer in the industrialized world, with an annual death toll exceeding 31,000 in the United States.

When Panc-1 cells are treated with SPC, a reorganization of keratin into a perinuclear ring-like structure begins at about 15 min and reaches its stable configuration at around 45 min. Phosphorylation of keratin has been correlated with the reorganization of keratin following SPC treatment of Panc-1 cells [16]. Fig. 1(a) shows a phase contrast image of Panc-1 cells in culture. Fig. 1(b) and (c) show immuno-fluoroscence images of the effects of SPC treatment on the keratin cytoskeleton assembly in Panc-1 cells at 0 min and 60 min without and with SPC treatment, respectively. Enlargement of the cell areas which are marked by the two white boxes are shown on top of the respective images at 6 min intervals. Fig. 1(d) is a plot of normalized distance between the edge of the keratin intermediate filament distribution marked by fluorescence in Fig. 1(b) and (c) and the center of the Panc-1 cell for cases without (blue line) and with (red line) SPC treatment as a function of time. The SPC treatment leads to a marked increase in the density of perinuclear keratin filaments.

2.2. Effects of SPC on the mechanical response of Panc-1 cells

The connection between single cell elasticity and molecular reorganization induced by SPC in Panc-1 cancer cells was investigated by means of the mechanical microplate stretcher method, which is described in detail in Refs. [14–16]; information pertinent to the present work is summarized in the supplementary material S1 appended to this manuscript. Briefly, a single Panc-1 cell is placed in between two glass microplates coated with fibronectin, a known cell adhesion ligand. After adhesion between the cell and the surfaces of the microplates becomes well developed (after ~45 min), the microplates are moved apart by imposing a controlled displacement at a specific deformation rate, which results in the tensile stretching of the cell. These cell-stretching experiments are performed in a 30 ml chamber filled with high glucose DMEM (Dulbecco's modified Eagle's medium) supplemented with 2 mM L-glutamine at 37 °C. The resistance to elastic deformation of the cell along with the stiffness of the loading system gives rise to a maximum force, on the order of several hundred nanoNewtons. The effective spring constant of the cell in units of micronewtons per meter, which is a measure of its elastic modulus, is then deduced from the force and displacement record. A feedback control system achieves displacement control wherein the instantaneous displacement value is compared with the set value every 100 ms. Depending on the sign of the difference between the actual and set value, one microplate is displaced with respect to the other in increments of ±50 nm. The attendant control rate is 0.5 $\mu m\,s^{-1}$ and is kept constant for all experiments.[3] The final displacement rate is dictated by the biophysical state of the cell, including adhesion between the cell and the microplates. The entire experimental set up was placed in a box where the temperature was controlled to be at a fixed value of 37 °C. Supplementary material S2 appended to this paper includes a video clip of tensile loading and unloading cycles of Panc-1 cells.

Fig. 2(a) shows the tensile displacement imposed on the Panc-1 cell as a function of time and the simultaneous measurement of resultant force, also as a function of time. The zero force value for the measurement was determined when the cell lost contact with one of the microplates, thereby unloading flexible microplate (force sensor) at the end of the experiment. The tensile displacement (plotted in black color) is periodic. The displacement cycle with a period of approximately 5 min is composed of a linear increase to 5 μm, then a linear decrease at the same rate to the initial reference level, and finally a rest period of 2.5 min at the end of the cycle. Six such displacement cycles are imposed on the cell so as to stabilize the initial deformation and the adhesion between the cell and the microplates. The resultant force response of the cell as a function of time is also plotted in Fig. 2(a) in green color.

After the initial period of 35 min (which corresponds to the time period for six displacement cycles separated by rest periods), the Panc-1 cell is treated with 10 μM concentration of SPC. Upon addition of SPC, the cycle duration is extended to approximately 7 min for 7 cycles before reverting to the original loading conditions after the SPC has reacted with the cell for 45 min (i.e., about 80 min after the commencement of the experiment). It is evident from Fig. 2(a) that the introduction of SPC causes a pronounced decrease in the force amplitude at fixed displacement amplitude, indicating softening of the elastic response of the SPC-treated Panc-1 cell, as well as relaxation processes upon linear decrease of displacement. As the cell settles into a cyclic deformation response, its effective displacement rate reaches a mean value of $0.065 \pm 0.005\,\mu m\,s^{-1}$ after SPC treatment, which is about 1.7 times greater than that without SPC. This indicates that the same control steps (50 nm displacement each 100 ms) impose 1.7 times greater effective displacement on the cell, ostensibly due to its softening after SPC treatment.

The initial drift to lower force values compensates for the manner in which adhesion of cell to the microplates adapts to the constraint. This change of adhesion occurs on a much longer time scale than the time needed for elastic probing of the cell. This is why force drift arising from cell adhesion does not contribute substantially to the evaluation of cell's mechanical properties obtained by the present short time force probing.

Fig. 2(b) shows the force versus displacement variations at different time periods from the information provided in Fig. 2(a). Several trends are seen from this figure. (i) Prior to the introduction of SPC, the force–displacement curves (plotted as black lines) show a similar response during the first six cycles, with little hysteresis. There is a small progressive drift, with time, of the force values toward lower levels during the displacement cycles. The inset in the top row of Fig. 2(b) schematically shows the keratin molecular network spanning the entire cytoplasmic region inside the stretched epithelial cell. (ii) Upon treatment with SPC, the force to sustain a given tensile displacement of the cell decreases, as shown in the lower row of Fig. 2(b) in blue color. (The jumps in force are a consequence of the changes in adhesion of the cell to the microplates during the rest periods.) In addition, the energy dissipation associated with the cyclic displacement loops, as given by the enclosed areas of the force–displacement plots, increases with time after SPC treatment, until a stable condition is reached after about 80 min. This change of elastic response of the cell and the concomitant increase in the energy dissipation accompany a reorganization of the keratin network, as schematically sketched in the inset appended to the lower row of Fig. 2(b).

Fig. 3 shows the effect of SPC on effective spring constant of Panc-1 cell and on hysteretic energy expended during displacement cycling in the mechanical stretcher. The elastic stiffness decreases by a factor of three from SPC treatment while energy dissipated per displacement cycle at 37 °C increases from near-zero levels to a saturation value. (Note that the dissipated energy per cycle per unit volume of the cell is given here in units of $k_B \cdot T\,\mu m^{-3}$ where k_B is the Boltzmann constant, T is the absolute temperature and the cell diameter was taken to be 22.3 μm; the cell was approximated as a sphere for the calculation of volume.) Both effects appear to have their origin in the phosphorylation of keratin and the attendant reorganization of the keratin molecular structure due to the introduction of SPC. One possible rationale for the increase in energy dissipation seen in the force–displacement plots is that SPC causes perinuclear reorganization of the molecular keratin, thereby depleting the rest of the

[3] The effective elastic response of the cell is known to be sensitive to the loading rate, based on experiments performed over a range of displacement rates between 0.5 and 2.0 $\mu m\,s^{-1}$ [16]. In the present discussion, we confine attention to a single stretching rate. The absolute value of cell stiffness depends on the deformation rate, although the trends reported here are unaffected by the specific rate of deformation.

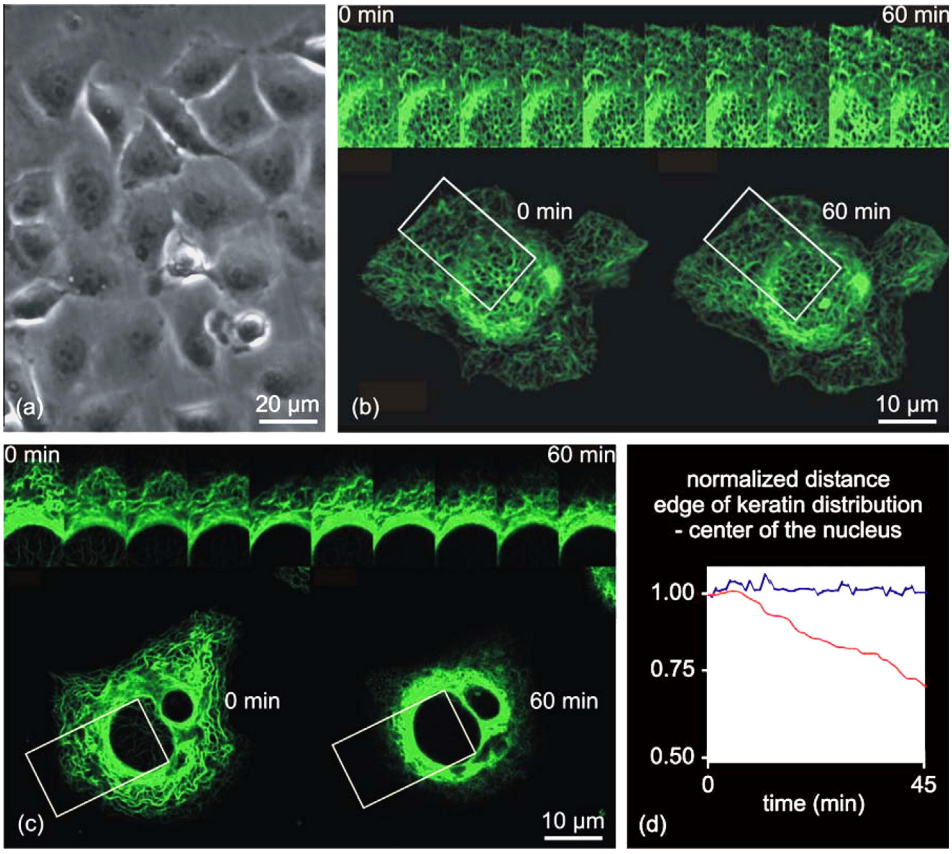

Fig. 1. Treatment of Panc-1 cells with SPC causes significant reorganization of the keratin filaments within the cell. (a) Phase contrast image of Panc-1 cell in culture. (b) and (c) Panc-1 cells were transfected with C-HK18-EYFPN1 (0.5 μg/ml) using Fugene 6 (Roche) and kept in dye-free DMEM (20 mM Hepes) in the presence or absence of 10 μM SPC. Images were taken using an Olympus Flowview 300 inverted confocal microscope (100×) with pre-heated stage kept at 37 °C over a period of 60 min. Cells are shown either prior to and 60 min after the addition of solvent (top panel) or SPC (bottom panel). The rectangular boxes show cell areas which are enlarged on top of the respective images for every 6 min. (d) Variation of distance between the edge of the keratin cytoskeleton distribution marked by fluorescence in (b) and (c) and the center of the Panc-1 cell nucleus for cases without (blue line) and with (red line) 10 μM SPC treatment as a function of time.

cytoplasm of keratin. As a result, a greater volume of the cell interior comprising the internal fluid could undergo viscous deformation than in the control condition. This could result in greater viscous energy dissipation that is manifested as increasing hysteresis loop area. It is also possible that the cell utilizes its own energy source to resist deformation imposed on it. However, if such deformation occurred due to active cell response, it would have been evident during rest periods in Fig. 2(a), which was not the case. Pinpointing the mechanistic reasons for the observed increase in energy dissipation per cycle would inevitably require additional studies of the full spectrum of frequency-dependent viscoelastic deformation response.

2.3. Effects of LPA on deformation of Panc-1 cells

SPC-induced keratin molecular rearrangement occurs independently of other cytoskeletal components such as F-actin and microtubules. For the present set of experiments, it appears that the effect on elastic modulus of SPC can be attributed primarily to changes in keratin molecular structure and not to any possible changes in actin or microtubules. We demonstrate this here through new force-control experiments wherein the Panc-1 cancer cell is treated first with 10 μM concentration of lysophosphatidic acid acid[4] (LPA) for 15 min instead of SPC; this is followed by SPC treatment.

The choice of LPA to alter the cytoskeleton structure, instead of treating the cell with SPC, is motivated by the fact that LPA facilitates the formation of actin stress fibers, instead of inducing a molecular reorganization of keratin. Thus, by comparing the effects of LPA with those of SPC on the elastic and viscoelastic responses of the Panc-1 cells, it would be feasible to discern whether the trends seen in Figs. 2 and 3 arise primarily as a result of keratin reorganization or whether these mechanical property changes are influenced by possible contributions from cytoskeletal components such as actin fibers.[5] We employ force-controlled stretching of the cell (instead of the displacement-controlled loading for the results plotted in Fig. 2) to illustrate the generality of the observed trends that are independent of the type of loading.

Fig. 4(a) shows a plot of force as a function of time under repeated tensile stretching (positive force values) and compression (negative force values) of the Panc-1 cell in force control; the corresponding evolution of displacement with time is also plotted. After initial deformation involving 12 force cycles over a period of 35 min, the Panc-1 cell was treated with LPA while mechanical deformation is continued. Subsequently, SPC is also added to the cell. It is evident from Fig. 4(a) that LPA has no significant effect on the elastic stiffness of Panc-1 cells (it seems only to increase very slightly the stiffness beyond the experimental scatter levels). However, when SPC is added at about 120 min, effective elastic

[4] LPA is also known to mediate a wide variety of biological processes including platelet activation, alteration of neuronal cell shape, mitogenesis and smooth muscle contraction [24].

[5] Elasticity of plasma membranes of endothelial cells, as measured using fibronectin-coated magnetic beads attached to the cell surface, is strongly influenced by stimulating agents such as thrombin [25], although LPA changes the elasticity of the membrane only slightly.

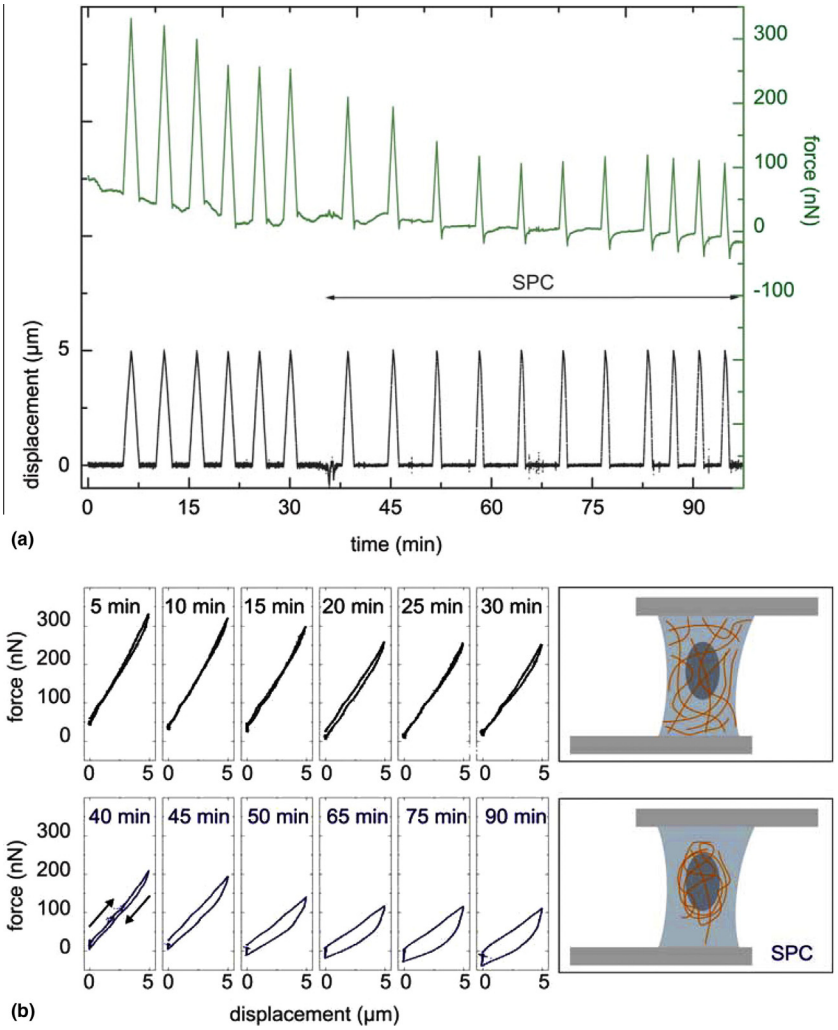

Fig. 2. SPC treatment significantly alters the elastic response and hysteretic energy dissipation of Panc-1 cancer cells subjected to repeated tensile stretching at a constant rate of 0.5 μm s^{-1}. (a) Displacement-controlled loading and unloading over six cycles spanning 35 min, following which the cell was treated with 10 μM SPC and the cycling continued. Imposed displacement is plotted against time in black color. The resulting force on the cell in response to displacement cycles is plotted (in green) as a function of time. (b) Force versus displacement hysteresis loops from the information in (a), at specified time intervals, before (black loops) and after (blue loops) SPC was added to cell. The drift in force is partially due to the adhesion and reaccommodation of the cell between the microplates. The top inset shows the schematic of the cell between the microplates where the keratin spans the entire volume of cytoplasm. The bottom inset shows the keratin altered by SPC so that it is confined to the perinuclear region. The arrow in (b) indicate the sense of the hysteresis loop.

constant of the cell markedly decreases as seen by the near doubling of the displacement at a fixed force level.

Fig. 4(b) shows force–displacement plots obtained from the data in Fig. 4(a) at specific time intervals. Deformation before LPA treatment of Panc-1 cell (black lines), after the introduction of 10 μM concentration of LPA only (purple lines), and after subsequent introduction of 10 μM concentration of SPC (blue lines) are indicated. LPA treatment does not lead to any noticeable change in the quasi-linear force–displacement relation or in the hysteresis loops. However, introduction of SPC at 120 min significantly increases elastic compliance and causes marked increase in dissipated energy (area of hysteresis loop). Remarkably, tensile stretching (positive force value) and compression (negative force values) show linear force–displacement relations with differences in elasticity. Unlike the case of tensile stretching, the effective elasticity obtained during cell compression is constant for all measurements which might indicate that the cell nucleus contributes to deformation. Thoumine and coworkers [27] treated the cell nucleus as an elastic object. Assuming that the elastic response of the nucleus is not affected by treatment with either LPA or SPC, one would expect a distinct difference between the deformability of the cell in tension and compression; this is indeed found to be the case in Fig. 4(b).

Variations of elastic spring constant and dissipated energy per cycle per unit volume as a function of time and with LPA and SPC treatment of Panc-1 cell are plotted in Fig. 5. LPA induces a small increase in stiffness, whereas SPC causes a threefold reduction in stiffness. Furthermore, changes to the actin fiber structure induced by prior treatment with LPA (which does not modify keratin) appear to have no bearing on the effects of SPC in reducing the elastic modulus of cell by reorganizing keratin. Enhancement in energy dissipation due to the structural reorganization of keratin by SPC to the perinuclear region of the cell is also seemingly unaffected by a priori LPA treatment.[6] The difference in absolute energy values at saturation between Figs. 5 and 3 is most likely due to differences in mechanical prehistory imposed on the cell.

[6] While there is no change in cell size for SPC and LPA treatments, the addition of LPA provides a much more stable adhesion between the cell and the microplates than treatment just with SPC.

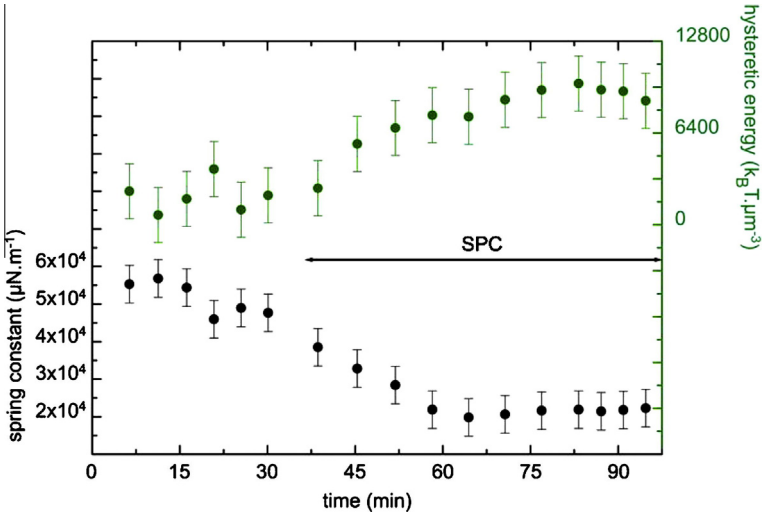

Fig. 3. Variation of the effective elastic spring constant of the cell stretched between the microplates as a function of time (black color filled circles with typical error bars). Note the threefold reduction in the elastic stiffness of the cell when the full effect of SPC treatment is realized. Also shown is the variation of energy dissipated per displacement cycle, computed from the area within the force–displacement loops such as those shown in Fig. 2(b), as a function of time. This is presented in units of k_BT, which is calculated for a temperature of 37.0 °C (k_BT = 0.0267 eV), per unit volume of the cell. Note the increase in energy dissipation upon addition of SPC.

2.4. Structure–property–oncogenic feature connection for gastrointestinal cancer cells

The results shown in Figs. 2–5 illustrate how structural changes to the intermediate filament network (i.e., keratin fibers) arising from a particular biochemical effect (i.e., treatment with SPC) can lead to marked changes in both elastic modulus (as seen in the significant reduction in cell spring constant) and changes in the area enclosed within force–displacement loops (as seen in the increase in energy dissipation per cycle per unit volume) of the Panc-1 cell. The results presented in this paper demonstrate that there occurs a significant increase in the hysteretic energy in force–displacement response of SPC-treated cell whereas no such trend is seen in LPA-treated cell.

The increased deformability of Panc-1 cancer cells due to SPC could increase migration probability of tumor cells through size-limited pores of basal membrane and endothelium. Penetration of cells through the endothelial layer is a critical step in cancer metastasis, which requires considerable elastic deformability of epithelial cells. We postulate here that the SPC-mediated reduction in elastic modulus and the significantly enhanced propensity of the cell to accommodate deformation through energy dissipation during repeated cell deformation, facilitate substantial, rapid and reversible "squeezing through" and migration of epithelial tumor cells through size limited pores.

Although the foregoing discussion pertains to Panc-1 pancreatic cancer cells, the mechanistic processes reported seem applicable to a broader range of epithelial tumors associated with the human gastrointestinal system. When a different model of epithelial cancer cells, i.e., human gastric adenocarcinoma cells (AGS) which also express K8 and K18 keratin, are treated with SPC, keratin reorganization results [15]. Perinuclear reorganization of keratin induced by SPC in AGS gastric cancer cells also leads to a decrease in elastic modulus, similar to that seen in Panc-1 cancer cells. However, when AGS cancer cells are treated with 10 μM LPA, the elastic modulus is found to increase by about 60%. These results indicate that SPC may also facilitate the movement of different types of epithelial tumor cells by enabling them to squeeze through membranous pores.

The experimental results presented here and in Ref. [16] do not appear to reveal any noticeable changes in the actin and microtubule fraction of the cytoskeleton. It is, however, generally known that subcellular networks are interconnected in such a way that changes in one component can affect the response of the other. For example, the coupling between actin cortex and intermediate filament based cytoskeleton can be markedly altered by cell activating agents such as histamine [26].

3. Mechanics of *Plasmodium*-harbouring RBCs

The human red blood cell (RBC) has a discocyte or biconcave shape and a diameter of 7.5–8.7 μm in its healthy state. It repeatedly undergoes large elastic deformation during its passage through small capillaries and the intercellular openings in sinusoids of the spleen over the course of its normal life span of 120 days. Among the four different species of *Plasmodium* (*P.*) with which human RBCs can be infected, *P. falciparum* and *P. vivax* are the most common, with the former resulting in more severe form of malaria [6]. Malaria induced by *P. falciparum* is the most widespread parasitic disease in humans with an estimated annual infection rate of several hundred million people worldwide and an estimated annual mortality rate of several million, mostly children. The disease state occurs when the parasite leaves the liver and invades RBCs, and during the subsequent asexual stage lasting about 48 h, the parasite multiplies inside the RBC producing up to 20 merozoites per parasite; each merozoite can subsequently invade other healthy RBCs.

When a merozoite invades an RBC, it undergoes pronounced structural changes within the RBC. The erythrocytic developmental stages of the parasite are broadly classified as: (i) the ring stage (with characteristic thin discoidal, flat or cup-shaped ring features whose formation commences at about 30 min from the time of penetration of the parasite into the RBC), (ii) trophozoite stage (with irregular bulges or knobs at the surface of the parasite appearing at about 20 h after invasion, parasite growth inside the RBC and formation of small pigmented regions), and (iii) the schizont stage (with nuclear division of the parasite resulting in the multiplication of the number of merozoites, greater spread of parasite and pigmented regions within cell volume, and export of parasite proteins to the RBC membrane causing severe distortion of the cell cytoskeleton and membrane some 25–40 h after invasion). In the late schizont stage, the infected RBC also exhibits a change in shape, which is spherical compared to the biconcave shape for the

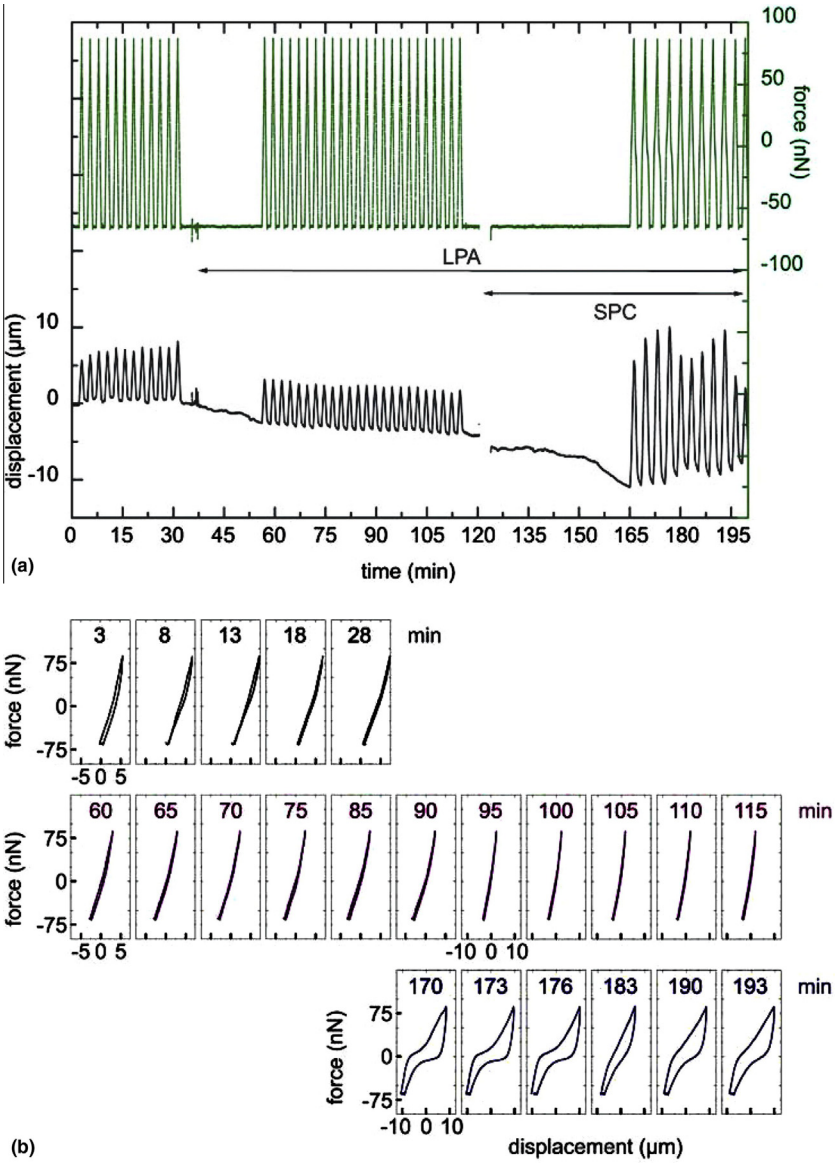

Fig. 4. Effects of LPA and SPC on mechanical properties of Panc-1 cells. (a) Repeated tensile force (green color) imposed on cell as a function of time, and resultant displacement (black) with time at a stretching rate of 0.5 μm s^{-1}. The cell was treated with 10 μM of LPA 35 min after onset of micromechanical assay, and additionally with SPC of the same concentration 85 min later. (b) Force versus displacement loops from the information in (a), at specified time intervals, for the cell deformed in DMEM with 2 mM L-glutamine before LPA treatment (black color), after LPA treatment (fucia color) and after SPC treatment (blue color).

healthy RBC. A review of structure evolution during these developmental stages can be found in Refs. [6,7,28].[7]

An important outcome of the full development of *P. falciparum* within the RBC is that it increases the adhesion of infected RBCs to inner linings of small blood vessels. Single-cell mechanical property measurements performed using the micropipette aspiration method [29,30] and the laminar shear flow method [8] also show that RBCs parasitized by *P. falciparum* stiffen considerably with marked increases in their elastic moduli. Profound alterations to the mechanical properties and adhesive response of the parasitized RBCs cause them to sequester in the microvasculature of major organs. Consequences of such sequestration could include cerebral malaria, hypoglycaemia, metabolic acidosis and respiratory distress [6].

By combining recent advances in nanotechnology with computational modelling, it is now possible to obtain direct force–displacement responses of living cells under direct tensile loading at pN-level forces. In this section, we present new results of direct force–displacement responses of RBCs parasitized by *P. falciparum* at different developmental stages. By integrating this information with related studies [18] on protein-specific contributions to RBC elasticity, we seek to establish some connections among protein structure, mechanical properties of infected cells and possible effects on disease progression.

3.1. Force–displacement curves for RBCs parasitized by P. falciparum

Mechanical response of RBCs has long been studied by means of the micropipette aspiration method (e.g., [5,31]) whereby a single cell is aspirated into a glass tube by application of suction pressure. From comparisons of geometry changes of the aspirated cell with that predicted from analytical and numerical models of deformation, its elastic response during the application of the pressure

[7] Infected RBCs (erythrocytes) continually transition between stages, which often makes identification of the exact stage of parasite development difficult. For results reported in this paper, we label cells clearly within one well-defined stage of parasite development.

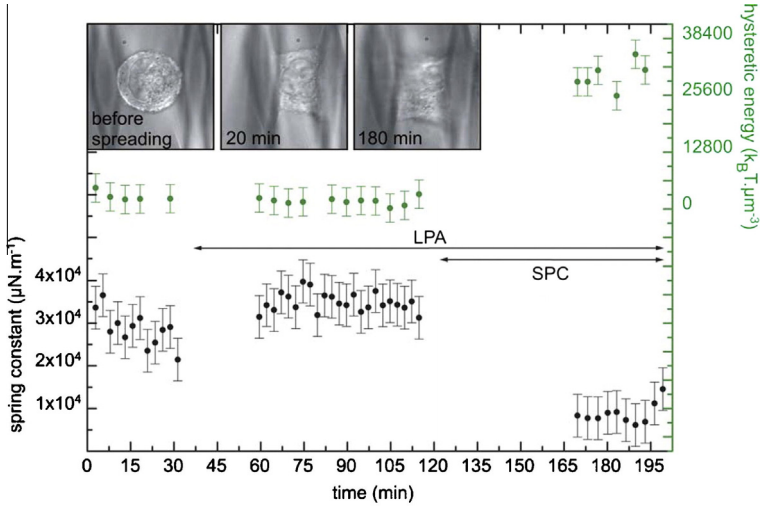

Fig. 5. Variation of the effective elastic spring constant of the cell stretched between the microplates as a function of time (black color filled circles with typical error bars). Note the threefold reduction in the elastic stiffness of the cell when the full effect of SPC treatment is realized, while LPA treatment has no significant effect on elasticity of cell. Also shown is the variation of energy dissipation per cycle per unit cell volume, computed from the area within the force–displacement loops such as those shown in Fig. 2(b), as a function of time, similar to Fig. 3. Note the increase in energy dissipation upon addition of SPC. The micrographs included with the figure show how the shape of the cell evolves due to adhesion with the microplates at the beginning of the experiment, at 20 min and at 180 min (upon treatment with SPC).

and its viscoelastic relaxation response upon release of pressure are estimated. Recently, direct tension loading of healthy RBCs has been achieved by employing the optical tweezers method [17,32–36], where two high refractive index beads attached to diametrically opposite ends of the cell can be moved apart relative to each other by optically trapping one or both beads with laser beams. By appropriately calibrating the stretching force and recording geometry changes during deformation by means of optical microscopy, variations of axial and transverse diameters of the cell with the stretching force are obtained. With proper choice of laser and silica beads (which serve as grips to load the cell in a phosphate-buffered saline (PBS) solution), recent studies [17] have demonstrated the feasibility to impose tensile stretching in large elastic deformation, with a force resolution as small as 1 pN. Full details of specimen preparation methods can be found elsewhere for optical tweezers stretching of healthy RBCs [17,32,34]. A brief summary of these methods is provided in supplementary material S3.

Experiments involved in vitro culturing of *P. falciparum* strains 3D7 [37] and Gombak A [38] using methods described previously [39] with appropriate modifications [40]. Cultures were grown at 5% hematocrit in 25 ml tissue culture flasks in a complete medium that consisted of RPMI 1640 supplemented with 4.2 ml/100 ml 5.0% $NaHCO_3$ and 0.5% w/v albumax (Gibco-BRL). Cultures were gassed with 3% O_2, 5% CO_2 and 92% N_2, and incubated at 37 °C in complete medium. Compared to the experimental methods employed for the optical tweezers stretching of healthy RBCs [17], the procedure for centrifugation and storage at 4 °C were omitted for the infected cells described here so as to reduce possible cell damage. The bonding of the silica beads to the cell membrane was naturally enhanced because of the increased adhesion of infected RBCs, without the need for centrifugation and refrigeration.

Two control conditions were employed: the healthy RBC (H-RBC) and RBC exposed to *P. falciparum* but uninfected (*Pf*-U-RBC). The different erythrocytic developmental stages of the *P. falciparum* parasite are hereafter referred to as *Pf*-R-pRBC (ring stage), *Pf*-T-pRBC (trophozoite stage) and *Pf*-S-pRBC (schizont stage). Fig. 6 shows optical images of the parasitized RBCs (*Pf*-R-pRBC, *Pf*-T-pRBC and *Pf*-S-pRBC) and the two control conditions (H-RBC and *Pf*-U-RBC) prior to in vitro stretching by optical tweezers at 25 °C in PBS solution (left column). The presence of the parasite is visible inside the three infected cells. Also shown in this figure are the deformed shapes of the cells at two different stretching forces: 68 ± 12 pN and 151 ± 20 pN.[8] At a fixed stretching force, the deformability of the parasitized cell is significantly reduced compared to that of the two control conditions. While *Pf*-R-pRBC and *Pf*-T-pRBC exhibit some noticeable deformability at both load levels, little deformation is seen in *Pf*-S-pRBC. The deformation for *Pf*-U-RBC is slightly smaller than that for H-RBC. Videoimages of the stretching of a healthy and an infected RBC by optical tweezers are shown in supplementary material S4.

Fig. 7(a) shows the increase in the axial diameter of the RBC in response to large deformation stretching by optical tweezers for different *P. falciparum* infestation conditions. The decrease in the transverse diameter of the cell for the same five conditions is plotted in Fig. 7(b). The data in Fig. 7(a) and (b) thus provide continuous force–displacement curves for different erythrocytic developmental stages of the parasite. The experimental data (discrete data with error bars) indicate significant stiffening of the RBC with the maturation of the parasite from the ring stage to the trophozoite stage to the schizont stage; the increase in axial diameter and the decrease in transverse diameter with stretching force progressively diminish with the erythrocytic development of the parasite. There is evidence indicating that exo-antigens released from mature parasites which have not invaded the RBCs could increase the stiffness of exposed but uninfected RBCs [29,41]. Consistent with this expectation, our experiments show that the average stiffness of *Pf*-U-RBC is 8 $\mu N\,m^{-1}$ compared to the value of 5.3 $\mu N\,m^{-1}$ for H-RBC (see Fig. 8). In the schizont stage, the RBC has very little deformability in both axial and transverse directions.

[8] As discussed in detail in Ref. [17], considerable uncertainty and errors can be introduced in the calibration of stretching force imposed by optical tweezers due to bead size variations, resolution of the optical system used to estimate critical fluid velocity for bead dislodging from the laser trap when employing Stokes' flow method for calibration, uncertainty in the height of the trapped bead with respect to the reference plane or microscope stage, etc. Another source of uncertainly is the linear extrapolation above 88 pN of the variation of trapping force versus laser power; this linearity assumption is invoked in our calibration procedure [17]. Based on repeated calibrations and multiple cell testing, we estimate the maximum error in force values to be ±20 pN, with lower error levels at lower force values.

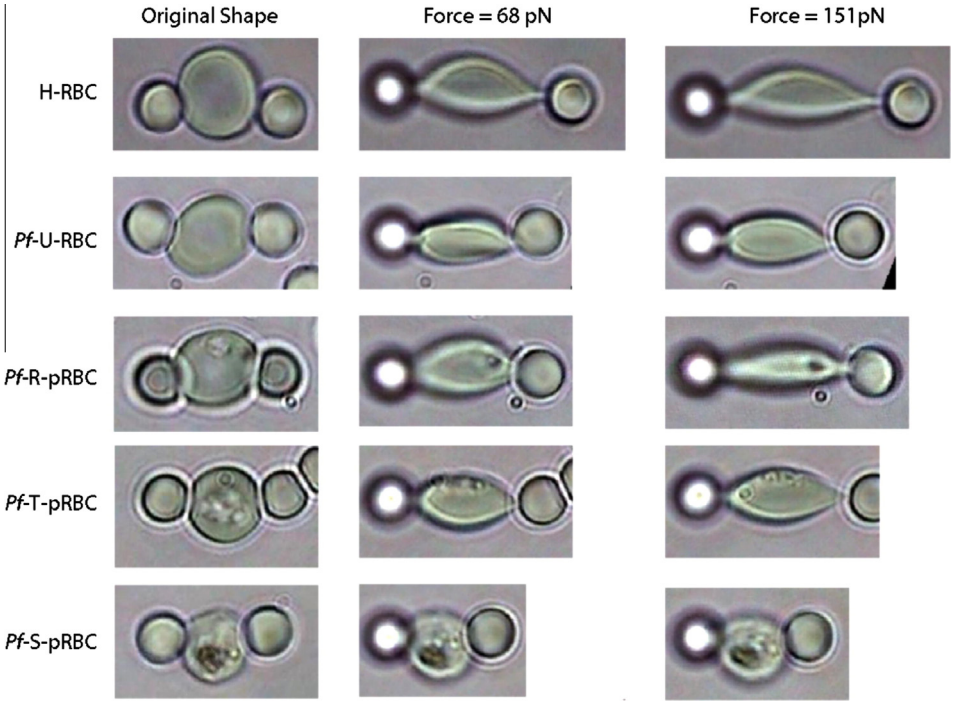

Fig. 6. Optical images of H-RBC, *Pf*-U-RBC, *Pf*-R-pRBC, *Pf*-T-pRBC and *Pf*-S-pRBC in PBS solution at 25 °C: prior to tensile stretching by optical tweezers (left column), at a constant force of 68 ± 12 pN (middle column) and at a constant force of 151 ± 20 pN (right column). Note the presence of the *P. falciparum* parasite inside the infected RBCs.

Superimposed on experimental data are simulated variations of axial and transverse diameters of the cell using a three-dimensional hyperelastic constitutive model incorporated into a finite element code. Details of the model along with descriptions of simulation methods are presented in Refs. [34,17] in the context of optical tweezers simulations of healthy RBCs. Further computational simulations of large deformation of healthy RBCs at the spectrin molecular level are considered in Ref. [36]. Supplementary material S5 summarizes the key features of computational analysis with additional references where further details can be found. Videoimages of the three-dimensional simulations of the deformation of a healthy RBC and an infected RBC stretched by optical tweezers are given in supplementary material S6.

3.2. Elastic modulus estimates for RBCs parasitized by P. falciparum

From the matching of computational results, shown by the dotted lines in Fig. 7(a) and (b) for the different infestation stages, with experimental data, the average shear modulus of the RBC was extracted. Fig. 8 shows the median value (marked by a small vertical line) and range of shear modulus values of the parasitized RBCs and the two control conditions, from the optical tweezers experiments and computational simulations. These values are based on repeat experiments conducted on 7, 8, 5, 5, and 23 samples for the H-RBC, *Pf*-U-RBC, *Pf*-R-pRBC, *Pf*-T-pRBC and *Pf*-S-pRBC conditions, respectively. Also shown in this figure are the shear modulus estimated from other independent experimental techniques involving micropipette aspiration [18] and laminar shear flow [8] for RBCs parasitized by *P. falciparum*. Several observations can be made from the information shown in Fig. 8 for RBCs infected with *P. falciparum*.

(1) The optical tweezers method is capable of providing the elastic deformation characteristics of the RBCs schizont stage infection, which prior methods [8,18,29,30] based on micropipette aspiration and laminar shear flow could not capture because of enhanced cell rigidity and increased cell adhesion.

(2) Estimates extracted from the present optical tweezers experiments point to substantially (by up to three to four times) greater stiffening of the RBCs from *P. falciparum* parasitization than previously anticipated [18]. The elastic shear modulus values for *Pf*-R-pRBC, *Pf*-T-pRBC, and *Pf*-S-pRBC are 16, 21.3 and 53.3 μN/m, respectively. The shear modulus of *Pf*-S-pRBC is up to an order of magnitude higher than that of H-RBC (median in-plane shear modulus, μN/m: H-RBC = 5.3, *Pf*-S-p-RBC = 53.3 (see Fig. 8); $p = 0.00011$).[9] The RBC infected with the parasite at the schizont stage also undergoes a shape change to a sphere compared to the biconcave (discocyte) shape of a healthy RBC. The spherical shape is also less conducive to severe deformation at large strains because of its weakened deformability (spherocytosis) due to lower surface to volume ratio and because its membrane does not fold as in the case of the discocyte shaped cell [17,34].

When the stretching force imposed on RBC is released, the cell fully relaxes to its original shape. From videoimages of such relaxation, the characteristic time of relaxation can be estimated. Optical tweezers studies of healthy RBCs [17,34] suggest that the characteristic relaxation time is 0.19 ± 0.06 s; corresponding literature value estimated from micropipette experiments is 0.10–0.30 s [5]. No significant differences in the viscoelastic response, over and

[9] The statistical significance of the differences between different cases was assessed by the *p*-value based on the Mann-Whitney U test. This value was evaluated at percent elongation in the axial direction at 108 pN of force, indicates the difference between two data sets based on their medians. In comparison of H-RBC and Pf-S-RBC, the low *p*-value (0.00011 < 0.05) shows statistically significant difference between the data sets. Comparing H-RBC to Pf-U-RBC, $p = 0.072$, which indicates that the medians are only very mildly distinct.

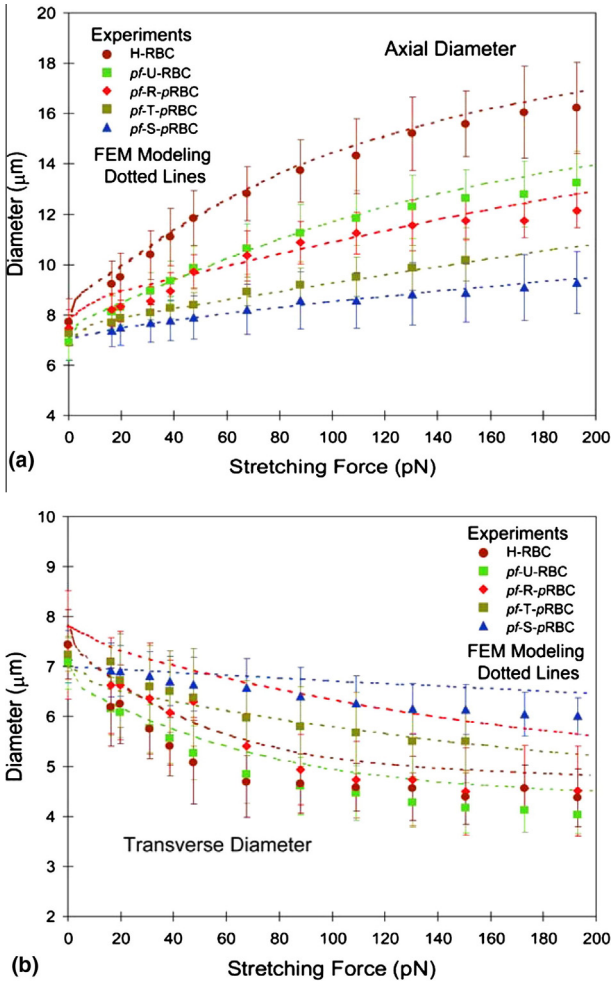

Fig. 7. Variation of (a) increase in axial diameter and (b) decrease in transverse diameter of the RBC with force from optical tweezers tests. Experimental data are indicated by discrete points with error bars in both figures. The maximum uncertainty in the reported stretching force is estimated to be ±20 pN. The scatter bands are based on repeat experiments with 7, 8, 5, 5 and 23 cells for the H-RBC, *Pf*-U-RBC, *Pf*-R-pRBC, *Pf*-T-pRBC and *Pf*-S-pRBC cases, respectively. The dotted lines denote predicted variations of axial and transverse diameters with stretching force, using the three-dimensional simulations.

above the experimental scatter, could be identified for the malaria-infected RBCs.

3.3. Some structure–property–biology connections for plasmodium-infected RBCs

The significant increase in the elastic stiffness of the human RBC due to parasitization by *P. falciparum* (Fig. 8) can arise partly from the presence of rigid parasites inside the cells which multiply by nuclear division in the late schizont stage to produce as many as 20 merozoites per mature parasite progeny. The continual structural changes occurring during the asexual blood stage of the parasite are also accompanied by changes to the cell membrane and cytoskeleton [6,7]. The study of hereditary haemolytic anaemia has long provided insights into the organization of sub-membranous cytoskeletal proteins and their molecular architecture [6,18], from which three broad inferences can be extracted: (1) protein–protein and protein–lipid interactions greatly influence the correct assembly of the membrane cytoskeleton, (2) the cortical skeleton mostly determines the discocytic shape of the RBC and its deformability, and (3) changes to the cytoskeletal chemistry and architecture can produce significant alterations to the RBC shape, elastic properties and rheological response.

In normal RBCs, membrane mechanical properties are mostly governed by the sub-membrane protein architecture whose principal components comprise alpha- and beta-spectrin, actin, proteins 4.1 and 4.2, adducin, dematin, protein 3 and its partner ankyrin. Attachments between the membrane and cytoskeleton are facilitated by chemical interactions involving ankyrin and the RBC anion transporter as well as protein 4.1 and glycophorin A [6,7,18]. Alterations to this delicate molecular architecture due to abnormalities that mediate cross-linking of cytoskeletal proteins can result in severe stiffening of the RBC. When the *P. falciparum* parasite develops inside an RBC, several parasite proteins are introduced into the RBC membrane and cytoskeleton, altering its mechanical response and adhesive properties. Among these proteins, *P. falciparum* ring-infected erythrocyte surface antigen (RESA) or Pf155 gets deposited into the cytoplasmic surface of the erythrocyte membrane from the dense granules in the apical region of the merozoite during parasite invasion. RESA associates with the spectrin network underneath the RBC membrane [41]. It has been suggested [36,42] that interaction of RESA with spectrin network possibly contributes to the increase in elastic modulus of parasite-harboring RBC during ring stage of parasite development.[10] In addition to RESA, knob-associated histidine-rich protein (KAHRP) and *P. falciparum* erythrocyte membrane protein 3 (PfEMP3) are exported from the parasite to the RBC membrane. Methods to knock out either KAHRP or PfEMP3 with transgenic parasite clones have also provided means for systematically characterizing the individual contributions to the increase in modulus of malaria-infected RBC from specific proteins. Fig. 9 shows the RBC shear modulus for the H-RBC, *Pf*-U-RBC, as well as for RBC parasitized by knobby clone (3D7), by knobby clone with PfEMP3 knocked out (EMP3KO) and by knobless KAHRP knockout clone (KKO), obtained by Glenister et al. [18] using micropipette aspiration measurements. It is seen that when either KAHRP or PfEMP3 is deleted from the cell membrane, the elastic modulus decreases by about 50% and 15%, respectively. Limited experimental data from the micropipette aspiration appear to indicate that loss of RESA expression does not appreciably alter the deformability of *Plasmodium*-harbouring RBCs at the trophozoite stage [44].

The pronounced increase in rigidity of RBCs infected with *P. falciparum* has important consequences for biological functions. RBCs coated with an antibody or having impaired deformability due to membrane proteins or intracellular particulates may be removed by the spleen. RBCs parasitized by *P. falciparum* adhere to vascular endothelium during developmental stage (between about 13 and 24 h after invading RBC), thereby avoiding removal by spleen [45,46]. Thus, how *P. falciparum* development in the RBC leads to severe malaria could be partially linked to changes in RBC mechanical properties in addition to other pathogenic components such as uncontrolled systemic inflammatory process.

To illustrate this connection, we compare effects on RBC deformability of *P. falciparum* with those of *P. vivax*. Although both species of *Plasmodium* are equally prevalent in Southeast Asia, the former is responsible for essentially all malaria-related mortality whereas the latter is relatively benign. Experiments [8] with laminar shear flow method reveal that deformability of human RBCs parasitized by *P. vivax* is greater than that of healthy RBCs (with the modulus of RBC infected to amoeboid stage decreasing by 50% from that of H-RBC), in contrast to behavior exhibited by RBCs infected with *P. falciparum*.

[10] Even if the parasite is eliminated from the RBC by the spleen, or it degrades within the RBC, the survival of the parasite-free RBC could be shortened due possibly to reduced deformability even after the removal of the parasite from the cell because of remnant RESA [43].

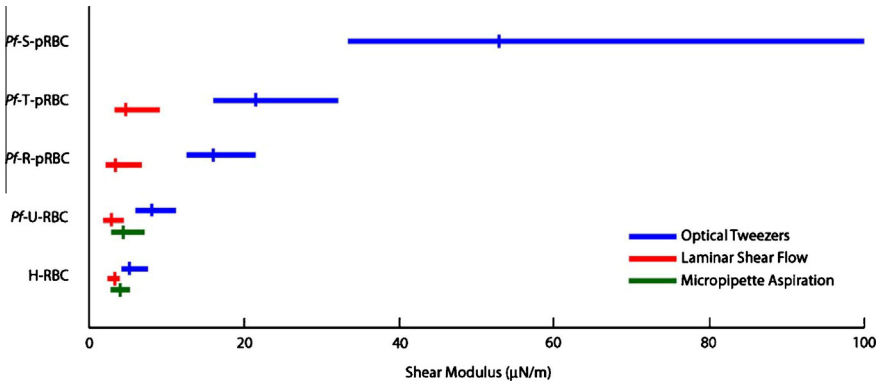

Fig. 8. Effective values of the in-plane shear modulus of the RBC membrane comprising the lipid bilayer and spectrin network, estimated from the present optical tweezers experiments and computational simulations of RBCs infected with *P. falciparum*. Also shown in this figure for comparison purposes are shear modulus estimates from micropipette aspiration [18] and laminar shear flow [8] methods, for parasitized RBCs at different developmental stages of *P. falciparum*.

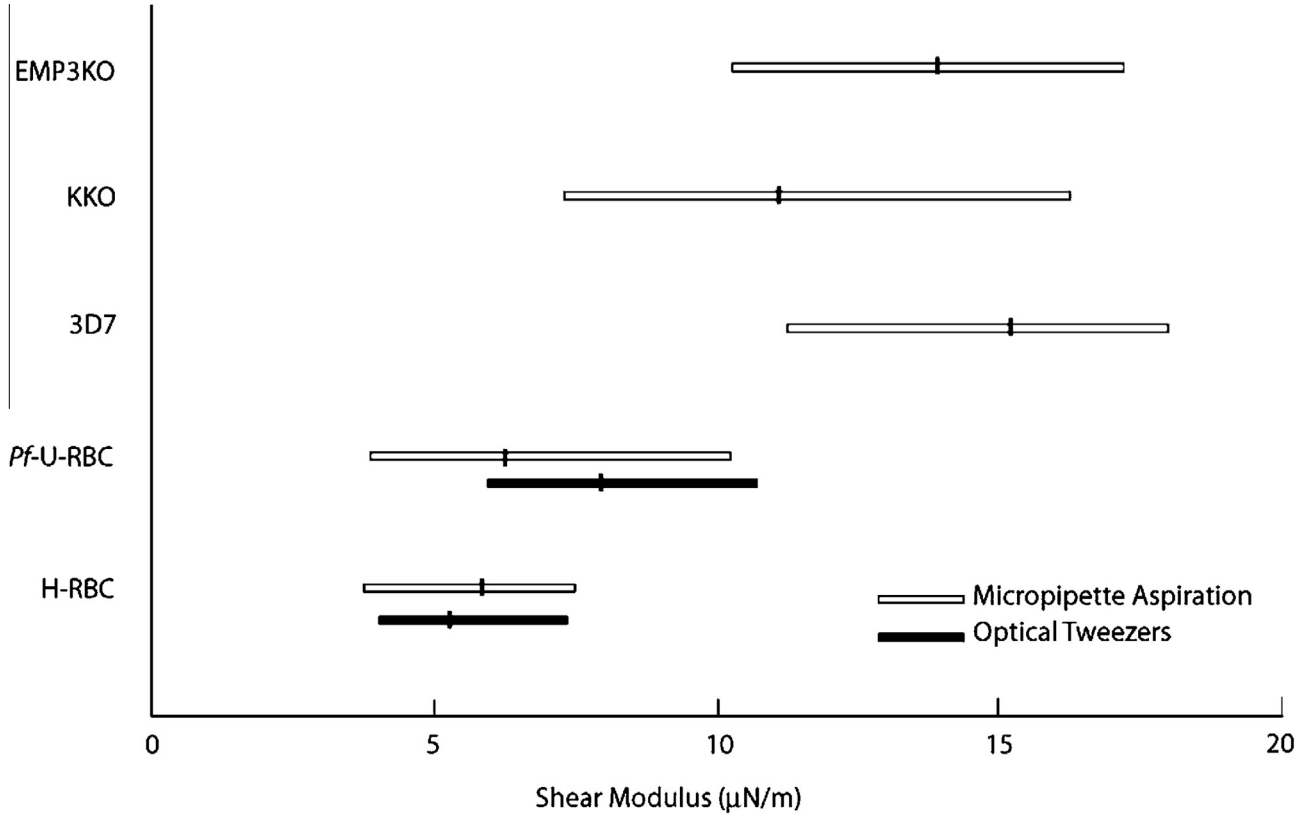

Fig. 9. Average and range of values of effective shear modulus of the human RBC parasitized by knobby clone (3D7), by knobby clone with PfEMP3 knocked out (EMP3KO) and by knobless KAHRP knockout clone (KKO). Also shown are the control conditions H-RBC and *Pf*-U-RBC. Data from micropipette aspiration measurements [18] superimposed with data for uninfected cells from the present optical tweezers experiments.

Furthermore, the surface area of RBC infected by *P. vivax* to a mature stage is double that of a healthy RBC. These results point to the possibility that by increasing its deformability and surface area significantly upon invasion by *P. vivax*, the infected young RBCs (reticulocytes) are able to circulate unhindered through the intercellular gaps in the sinusoids of the spleen, thereby avoiding splenic entrapment.

4. Concluding remarks

In this paper, we have demonstrated some connections among molecular structure, single-cell mechanical properties and biological functions in the context of two very different human diseases. For this purpose, we have performed single-cell mechanical deformation experiments on gastrointestinal epithelial tumor cells and *Plasmodium*-harbouring human red blood cells. These specific cases, in conjunction with our parallel work and recent literature results, point to some mechanistic pathways, commonalities and differences associated with (a) the influence of biochemical factors on intracellular molecular reorganization, (b) the effects of structural changes on clear transitions in elastic and/or viscoelastic response, (c) the possible role of changes in mechanical properties in determining shape changes and mobility of the cell, and (d) the effects of cell mobility on the progression and severity of the disease.

For the subline of pancreatic cancer cells, Panc-1, naturally occurring bioactive lipid SPC which is known to influence cell proliferation, cell migration and cancer metastasis, is also found to

cause significant reorganization of keratin molecular network to perinuclear region of the cell. For both displacement- and force-controlled probing, we show a threefold reduction in elastic modulus of SPC-treated cell and a marked concomitant increase in energy dissipation during cyclic tensile deformation. The latter effect accompanies depletion of keratin from the bulk of cytoplasm due to SPC-induced molecular rearrangement. If the Panc-1 cell is treated with LPA (which does not reorganize keratin), instead of SPC, little change in either elastic response or hysteretic energy dissipation is observed. We postulate that keratin-induced structural changes, the ensuing mechanical property changes and energy dissipation processes facilitate easier migration of epithelial tumor cells through size-limited openings of basal membrane and the endothelium (which is deemed a critical step in cancer metastasis). This inference is additionally consistent with the experimental finding [16] that a different model of the gastrointestinal epithelial cells, i.e., the gastric adenocarcinoma cells (AGS), which also undergoes SPC-induced keratin reorganization to the cell perinuclear region, exhibits elastic property changes similar to those of Panc-1 tumor cells.

For the case of human RBCs parasitized by *P. falciparum*, we show up to a 10-fold increase in elastic stiffness in the advanced stages of intracellular parasite development compared to the healthy RBCs. By employing state-of-the art nanomechanical probes, we present here the first continuous and direct force versus displacement curves for the parasite-harbouring RBC as a function of the developmental stage of the parasite. In contrast to the gastrointestinal epithelial tumor cells, the parasite-harbouring RBCs, which are significantly stiffened by *P. falciparum* infestation, sequester in the microvasculature contributing to organ failure. The stiffening effect is ascribed to specific proteins transported from the parasite surface to the cell membrane and possible contributions to stiffening from such proteins are examined from recent results [28]. This possible connection between molecular structure and mechanical property is also seen to have important consequences for biological function and disease progression. When the RBCs are infected with *P. vivax*, instead of *P. falciparum*, the deformability as well as surface area of the cell is increased [8]. The RBC developmental stage subverted by *P. vivax* merozoites are reticulocytes. As a result, the *P. vivax*-harbouring RBCs are likely to circulate relatively easily through the intercellular gaps in the sinusoids of the spleen, thus circumventing the possibility of splenic entrapment.

The two cases of human diseases examined in this paper also point to the specific manner in which biochemical modifications of single cells can either increase or decrease the deformability of the affected cell. We show that whether this biochemically induced change in mechanical response is beneficial or detrimental from the viewpoint of disease progression is specific to the mechanisms involved. For the case of epithelial tumor cells, increased deformability may lead to an increased probability for cell mobility through basal membrane and endothelium thereby exacerbating cancer metastasis. On the other hand, reduced deformability of RBCs infected by *P. falciparum* can lead to increased sequestration in microvasculature, thereby worsening the severity of the disease. Such connections among structure, mechanical properties and biological function can provide critical insights into mechanisms of disease progression which have hitherto not been well understood. More complete knowledge of these connections also has the potential to offer new diagnostic tools and treatments.

Acknowledgments

S.S. acknowledges the Senior Humboldt Research Prize from Alexander von Humboldt Foundation, Germany, and an inter-university collaboration grant from the National University of Singapore, which provided partial funding to perform the research reported in this paper. He also thanks Drs. G. Milon and P. David of Institut Pasteur, Paris, for their helpful comments on this manuscript. J.S. and A.M. acknowledge the German Science Foundation (DFG, SP 520/5-1) and the Fonds der Chemischen Industrie. A.M. is also grateful for fellowship support from Région Rhône-Alpes (France). J.P.M. and C.T.L. are thankful to the Faculty of Engineering at the National University of Singapore for partial support of this research. Thanks are also due to Dr. Kevin Tan and Ms. Qie Lan of the National University of Singapore for assistance with the work on malaria-infected red blood cells, and to Deutsche Forschungsgemeinschaft (DFG)/SFB 518, the Interdisciplinary Center for Clinical Research (IZKF) at the University of Ulm and the Association for International Cancer Research.

Appendix A. Supplementary material

Supplementary material associated with this article can be found, in the online version, at doi:10.1016/j.actbio.2004.09.001.

S1. Experimental methods and materials for mechanical probing of Panc-1 cells.
S2. Video clip from the mechanical stretcher experiment showing a tensile loading and unloading cycle of the Panc-1 cell.
S3. Materials and Experimental Methods for Optical Tweezers Study of Healthy and Plasmodium-Infected Red Blood Cells.
S4. Videoimages from experiment of the stretching of healthy and infected RBCs by optical tweezers.
Video clip S4-1: This video clip is from an experiment of the large deformation stretching of a healthy RBC by optical tweezers.
Video clip S4-2: This video clip is from an experiment of the large deformation stretching of a *Pf*-S-pRBC cell by optical tweezers.
S5. Computational modeling of optical tweezers stretching of malaria-infected human red blood cells.
S6. Videoimages of computational simulations.
Video clip S6-1: Finite element simulation of a healthy RBC undergoing uniaxial stretching by optical tweezers. The video clip shows the shape evolution up to a maximum stretching force of 190 pN. The biconcave RBC's initial diameter was taken to be 7.8 μm, and the contact diameter with the bead chosen as 2 μm. The effective membrane shear modulus was assumed to be 4 μN/m, which represents the average modulus estimated from experiments on a number of healthy RBCs.
Video clip S6-2: Finite element simulation of a tophozoite-stage malaria-infected RBC under uniaxial stretching by optical tweezers. The video clip shows shape evolution up to a 190 pN load. The biconcave RBC's initial diameter was taken to be 7.8 μm, and the contact diameter with the bead chosen as 2 μm. The membrane shear modulus was assumed to be 16 μN/m in this simulation, which represents the average modulus estimated from experiments on a number of *Pf*-T-pRBC cells.

References

[1] Fuchs E, Weber K. Intermediate filaments: structure, dynamics, function and disease. Ann Rev Biochem 1994;63:345–82.
[2] Bao G, Suresh S. Cell and molecular mechanics of biological materials. Nature Mater 2003;2:715–25.
[3] Ingber DE. Mechanical signalling and cellular response to extracellular matrix in angiogenesis and cardiovascular physiology. Circ Res 2002;91:877–87.
[4] Alberts B et al. Molecular biology of the cell. 4th ed. New York: Garland; 2002.

[5] Boal D. Mechanics of the cell. Cambridge, UK: Cambridge University Press; 2002.
[6] Miller LH, Baruch DI, Marsh K, Doumbo OK. The pathogenic basis of malaria. Nature 2002;415:673–9.
[7] Cooke BM, Mohandas N, Coppell RL. The malaria-infected red blood cell: structural and functional changes. Adv Parasitol 2001;50:1–86.
[8] Suwanarusk R, Cooke BM, Dondorp AM, Silamut K, Sattabongkot J, White NJ, et al. The deformability of red blood cells parasitized by *Plasmodium falciparum* and *P. vivax*. J Infect Diseases 2004;189:190–4.
[9] Maniotis AJ, Chen CS, Ingber DE. Demonstration of mechanical connections between integrins, cytoskeletal filaments, and nucleoplasm that stabilize nuclear structure. Proc Natl Acad Sci USA 1997;94:849–54.
[10] Moyano JV, Maqueda A, Casanova B, Garcia-Pardo A. $\alpha 4\beta 1$ Integrin/ligand interaction inhibits $\alpha 5\beta 1$-induced stress fibers and focal adhesions via down-regulation of RhoA and induced melanoma cell migration. Mol Biol Cell 2003;14:3699–715.
[11] Bausch AR, Möller W, Sachmann E. Measurement of local viscoelasticity and forces in living cells by magnetic tweezers. Biophys J 1999;76:573–9.
[12] Van Vliet KJ, Bao G, Suresh S. The biomechanics toolbox: experimental approaches to living cells and biomolecules. Acta Mater 2003;51:5881–905.
[13] Guck J, Ananthakrishnan R, Mahmood H, Moon TJ, Cunningham CC, Käs J. The optical stretcher: A novel laser tool to micromanipulate cells. Biophys J 2001;81:767–84.
[14] Thoumine O, Ott A. Time scale dependent viscoelastic and contractile regimes in fibroblasts probed by microplate manipulation. J Cell Sci 1997;110:2109–16.
[15] Thoumine O, Ott A, Cardoso O, Meister JJ. Microplates: a new tool for manipulation and mechanical perturbation of individual cells. J Biochem Biophys Meth 1999;39:47–62.
[16] Beil M et al. Sphingosylphosphorylcholine regulates keratin network architecture and visco-elastic properties of human cancer cells. Nature Cell Biol 2003;5:803–11.
[17] Mills JP, Qie L, Dao M, Lim CT, Suresh S. Nonlinear elastic and viscoelastic deformation of the red blood cell induced by optical tweezers. Mech Chem Biosyst 2004;1:169–80.
[18] Glenister FK, Coppel RL, Cowman AF, Mohandas N, Cooke BM. Contribution of parasite proteins to altered mechanical properties of malaria-infected red blood cells. Blood 2002;99:1060–3.
[19] Liliom K et al. Sphingosylphosphocholine is a naturally occurring lip mediator in blood plasma: a possible role in regulating cardiac function via sphingolipid receptors. Biochem J 2001;355:189–97.
[20] Rodgriguez-Lafrasse C, Vanier MT. Sopphingosylphosphorylcholine in Niemann—Pick disease brain: accumulation in type A but not in type B. Neurochem Res 1999;24:199–205.
[21] Xiao YJ. Electrospray ionization mass spectrometry analysis of lysophospholipids in human ascitic fluids: comparison of the lysophospholipid contents in malignant vs nonmalignant ascitic fluids. Anal Biochem 2001;290:302–13.
[22] Desai NN, Spiegel S. Sphingosylphosphorylcholine is a remarkably potent mitogen for a variety of cell lines. Biochem Biophys Res Comm 1991;181:361–6.
[23] Boguslawski G, Lyons D, Harvey KA, Kovala AT, English D. Sphingosylphophorylcholine induces endothelial cell migration and morphogenesis. Biochem Biophys Res Comm 2000;272:603–9.
[24] Seufferlein T, Rozengurt E. Lysophosphatidic acid stimulates tyrosine phosphorylation of focal adhesion kinase, paxillin and p130. J Biol Chem 1994;269:9345–51.
[25] Bausch AR, Hellerer U, Essler M, Aepfelbacher M, Sackmann E. Rapid stiffening of integrin receptor-actin linkages in endothelial cells: Stimulated with thrombin: A magnetic bead microrheology study. Biophys J 2001;80:2649–57.
[26] Shasby DM, Ries DR, Shasby SS, Winter MC. Histamine stimulates phosphorylation of adherens junction proteins and alters their links to vimentin. Am J Physiol Lung Cell Mol Physiol 2002;282:L1330–8.
[27] Caille N, Thoumine O, Tardy Y, Meister JJ. Contribution of the nucleus to the mechanical properties of endothelial cells. J Biomech 2002;35:177–87.
[28] Bannister LH, Hopkins JM, Fowler RE, Krishna S, Mitchell GH. A brief illustrated guide to the ultrastructure of *Plasmodium falciparum* asexual blood stages. Parasitol Today 2000;16:427–33.
[29] Cranston HA, Boylan CW, Carroll GL, Sutera SP, Williamson JR, Gluzman IY, et al. *Plasmodium falciparum* maturation abolishes physiologic red cell deformability. Science 1984;223:400–3.
[30] Paulitschke M, Nash GB. Membrane rigidity of red blood cells parasitized by different strains of *Plasmodium falciparum*. J Lab Clin Med 1993;122:581–9.
[31] Evans E, Hochmuth RM. Membrane viscoelasticity. Biophys J 1976;16:1–11.
[32] Hénon S, Lenormand G, Richert A, Gallet F. A new determination of the shear modulus of the human erythrocyte membrane using optical tweezers. Biophys J 1999;76:1145–51.
[33] Sleep J, Wilson D, Simmons R, Gratzer W. Elasticity of red cell membrane and its relation to hemolytic disorders: an optical tweezers study. Biophys J 1999;77:3085–95.
[34] Dao M, Lim CT, Suresh S. Mechanics of the human red blood cell deformed by optical tweezers. J Mech Phys Solids 2003;51:2259–80.
[35] Lim CT et al. Large deformation of living cells using laser traps. Acta Mater 2004;52:1837–45. Also see. Corrig. Acta Mater 2004;52:4065–6.
[36] Li J, Dao M, Lim CT, Suresh S. Spectrin-level analysis of shape evolution and large deformation elasticity of erythrocyte. MIT Report Lexcom-2-04, Cambridge, MA, 2004.
[37] Walliker D, Quakyi IA, Wellems TE, Mccutchan TF, Szarfman A, London WT, et al. Genetic analysis of the human malaria parasite *Plasmodium falciparum*. Science 1987;26:1661–6.
[38] Ang HH, Lam CK, Wah MJ. In vitro susceptibility studies of *Plasmodium falciparum* isolates and clones against type II antifolate drugs. Chemotherapy 1996;42:318–23.
[39] Trager W, Jensen JB. Human malaria parasites in continuous culture. Science 1976;193:673–5.
[40] Smith TG, Lourenco P, Carter R, Walliker D, Ranford-Cartwright LC. Commitment to sexual differentiation in the human malaria parasite *Plasmodium falciparum*. Parasitology 2000;121:127–33.
[41] Foley M, Tilley L, Sawyer WH, Anders RF. The ring-infected erythrocyte surface antigen of *Plasmodium falciparum* associates with spectrin in the erythorocyte membrane-md. Biochem Parasitol 1991;46:137–47.
[42] Naumann KM, Jones GL, Saul A, Smith RA. *Plasmodium falciparum* exo antigen alters erythrocyte membrane deformality. FEBS Lett 1991;292:957.
[43] Newton PN et al. A comparison of the in vivo kinetics of *Plasmodium falciparum* ringinfected erythrocyte surface antigen-positive and -negative erythrocytes. Blood 2001;98:450–7.
[44] Diez Silva et al. Functional properties of the *Plasmodium falciparum* RESA proteinvsing transgenic parasites. Submitted for Publication, 2004.
[45] Dondorp AM, Kager PA, Vreeken J, White NJ. Abnormal blood flow and red cell deformability in severe malaria. Parasitol. Today 2000;16:228–32.
[46] Chotivanich K et al. Central role of the spleen in malaria parasite clearance. J. Infect. Diseases 2002;185:1538–41.